Extended EWMA Scheme for Enhanced Maxwell Process Monitoring: An Application to the Industrial Sector

Fuad S. Alduais[1,*]

[1]Department of Mathematics, College of Science and Humanities in Al-Kharj, Prince Sattam Bin Abdulaziz University, Al-Kharj, 11942, Saudi Arabia

Email: f.alduais@psau.edu.sa

Abstract

The neutrosophic framework offers a promising direction for modeling data affected by uncertainty. Many quality characteristics in the production industry follow the asymmetric structure of the Maxwell distribution. The neutrosophic VSQ chart serves as a novel tool for monitoring parameters of the neutrosophic Maxwell distribution. However, the existing structure of the neutrosophic VSQ chart, based on the basic Shewhart model, is generally unable to detect small shifts in the production process. In this study, a new control chart designed following the structure of the EWMA chart is developed to efficiently monitor Maxwell-distributed neutrosophic data. The run length properties of the proposed scheme are studied, and Monte Carlo simulations are performed to investigate its statistical characteristics. Numerical results indicate that the proposed chart is effective in detecting small shifts in the process. The practical utility of the proposed chart is demonstrated through a real-world industrial dataset affected by uncertainty.

Keywords: Control chart; Run length; Estimation; Simulation; Neutrosophic logic

1. Introduction

Statistical probability distributions are of central importance in Statistical Process Control (SPC) since they provide the basis for comprehension, modeling and the control of variability in industrial and service processes [1]. In SPC, the primary objective is to keep the process stable and within control limits [2]. It is possible to achieve this only if the natural statistical properties of process data are known, which is realized via probability distributions. For example, the normal distribution is often assumed in classical control charts such as the xbar, S and R charts in which process measurements are assumed to be normally distributed in the absence of process shift. The significance of asymmetric distributions in statistical applications and particularly in SPC lies in their ability to accurately model real-world data that deviates from the idealized assumption of normality [3]-[5]. But not all processes follow the normal distribution so, in some contexts, other distributions, such as the exponential, Weibull or gamma, or even more specific ones, such as Maxwell's or the inverse Gaussian, could apply [6]-[9]. These distributions enable researchers to capture skewed or heavy-tailed data more precisely, resulting in construction of more sensitive control charts and a more robust oddity detection system. In addition, probability distributions are utilized for the computation of important SPC measures such as the average run length (ARL), false alarm rates, and detection probabilities [10]. The distribution characteristics of process data should be understood in order to properly establish control limits and decrease the frequency of type I or type II errors. Furthermore, as noted in these works, inefficiently studying non-normal and non-simple data structures present in environments such as manufacturing, healthcare, and environmental monitoring is not acceptable in today's quality control practice, requiring application of flexible distributional assumptions to reasonably access process [11]. Maxwell control charts are important to statistical quality control and are appropriate for process monitoring whose data can be modelled by a Maxwell distribution, found in applications in the physical sciences and reliability [12]. These charts

DOI: https://doi.org/10.54216/IJNS.270215

enable the detection of shifts in the scale parameter of the underlying distribution, which corresponds, with changes in system or product performance [13]-[14]. Taking into consideration the special characteristics of the Maxwell-distributed data-including non-negativity and asymmetry of the data observations-Maxwell control charts result in more accurate and sensitive monitoring schemes than conventional Shewhart control charts. It results in better detection of process anomalies, better decision-making, and more effective wide range of industrial and scientific applications.

Control chart methodology based on data generating model, which is usually represented by some statistical distribution. Traditional statistical distributions, e.g. normal, exponential, Poisson, have limited capabilities, which are insufficient when addressing real-life situations where such elements as vague, or conflicting information are involved. Therefore, the incorporation of appropriate statistics distributions into SPC provides value added decision-making, facilitates process improvement, and contributes to product consistency. These classical models are also based on the belief that data is crisp and well defined, it behaves according to known probabilistic distribution which is actually not the case in many scenarios like uncertain decision making, ambiguous responses in survey, and noisy measurements of a sensor [15]-[17]. Hence, standard distributions are hard to fit for indeterminacy or partial ignorance, which in many cases entail inferences that are misleading or overly simplistic. To overcome these limitations, the neutrosophic probability distributions propose a more flexible model with three different aspects such as truth (T), indeterminacy (I) and falsity (F) whose value varies from 0 to 1 [18]-[22]. This triplet makes it possible to model uncertainty in a much richer and finer way than the traditional or the fuzzy model. For instance, consider the case where, due to sensor uncertainty or conflicting expert opinions, it may not be possible to unambiguously characterize a measurement as conforming or non-conforming: Neutrosophic distributions can capture and represent this indeterminacy effectively; a step that would have been discarded or wrongly modeled by classical mechanisms [23]. Recognizing and accepting the inherent inexactness and contradiction in data, neutrosophic probability distributions offer a more realistic and encompassing tool for statistical analysis [24]. They are particularly important in contemporary quality control, decision support systems and risk assessment models, as the use of standard distributions can introduce much practical inaccuracy. Hence, the proposition of neutrosophic distributions overcomes the defects of the classical distributions and enables the better working in uncertain and inconsistent environments.

In this work, we present the neutrosophic structure of MEWMA chart [13] to identify changes in the parameter of neutrosophic Maxwell distribution that is highly sensitive to minor changes.

The work is structured as follows. Section 2 explains some preliminary results related to neutrosophic Maxwell distribution. Section 3 discusses the proposed structure of EWMA chart for Maxwell distributed quality characteristic. Section 4 provides performance assessment of the proposed chart. Section 5 illustrates simulation setting for Maxwell data generating process and its monitoring under proposed chart. Section 6 demonstrates the applicability of the proposed chart for industrial data.

2. Neutrosophic Maxwell Distribution

In this section we discuss the basic structure of the Maxwell model with essential statistical characteristics. The Maxwell model with single parameter is given below:

$$h(z;\rho_N) = \sqrt{\frac{2}{\pi}}\,\frac{z^2}{\rho_N^3}\,e^{-z^2/(2\rho_N^2)},\ z>0 \qquad (1)$$

where Z is neutrosophic random variable and $\rho_N \in [\rho_l, \rho_u]$ is imprecise value of the neutrosophic Maxwell parameter. The neutrosophic probability Maxwell distribution function is a generalization of the classical Maxwell model for a level of uncertainty, indeterminacy, and vagueness by neutrosophic scale parameter. We can observe that the scale of the value is not presented as a fixed number, but as a neutrosophic number, that includes all possible values within an interval. The overall distribution shape is essentially unchanged from the classical Maxwell situation, the growth and the exponential fall-off continuing to balance each other. But using neutrosophic logic, the model is more flexible because in various practical situations the data might be blurred, measurements vague and parameters imprecisely known. It is then a straight thing this neutrosophic Maxwell distribution is extremely useful for application in, e.g., engineering, environmental science, medical diagnosis when decision in connection with incomplete or incomplete information has to be taken. In Figure. 1, the plot of with varied neutrosophic parameters for a continuous random variable is represented.

DOI: https://doi.org/10.54216/IJNS.270215

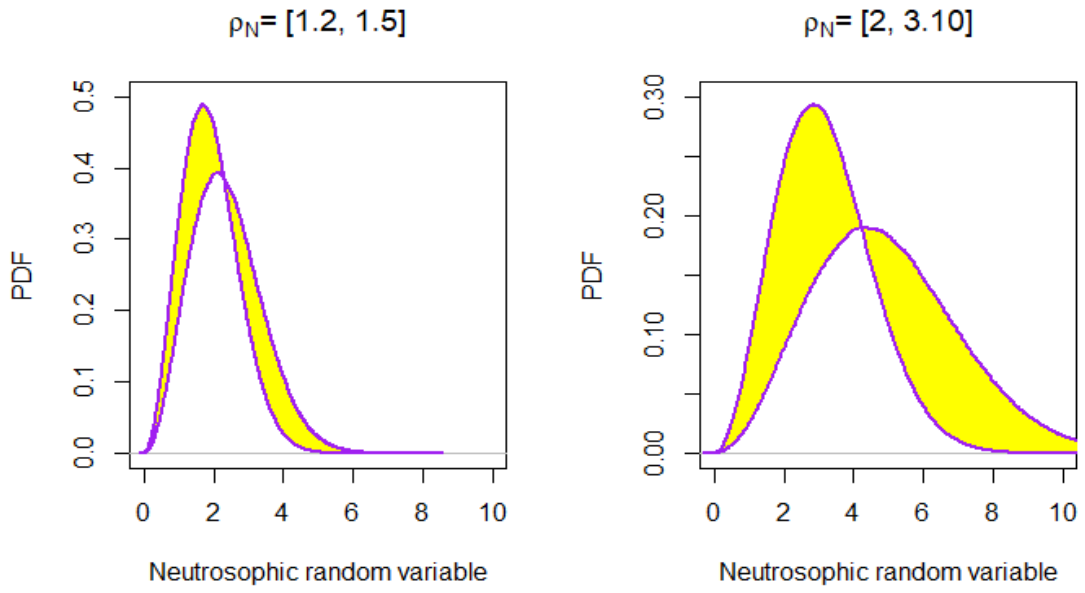

Figure 1. PDF plot of the neutrosophic Maxwell model at different values of ρ_N

The neutrosophic density function can reflect the probability that events occur between two reference points under the density curve. It is introduced in the framework of neutrosophic calculus as the integral of the variable density over a given interval. It represents only the scale factor whose various values generate several neutrosophic curves of the distribution being considered. The other related function of the PDF is the cumulative distribution function (CDF) which is given below:

$$H(z;\rho_N) = erf\left(\frac{z}{\sqrt{2}\rho_N}\right) - \sqrt{\frac{2}{\pi}}\frac{z}{\rho_N}\, e^{-z^2/(2\rho_N^2)},\ z > 0 \qquad (2)$$

The Maxwell distribution CDF describes the probability that a random variable is less than or equal to a specific value. This function is a product of the error function (erf) and an exponential term, representing the Gaussian shape and the positive support of the distribution, respectively. The CDF function with different values of neutrosophic scale parameter are shown in Figure 2.

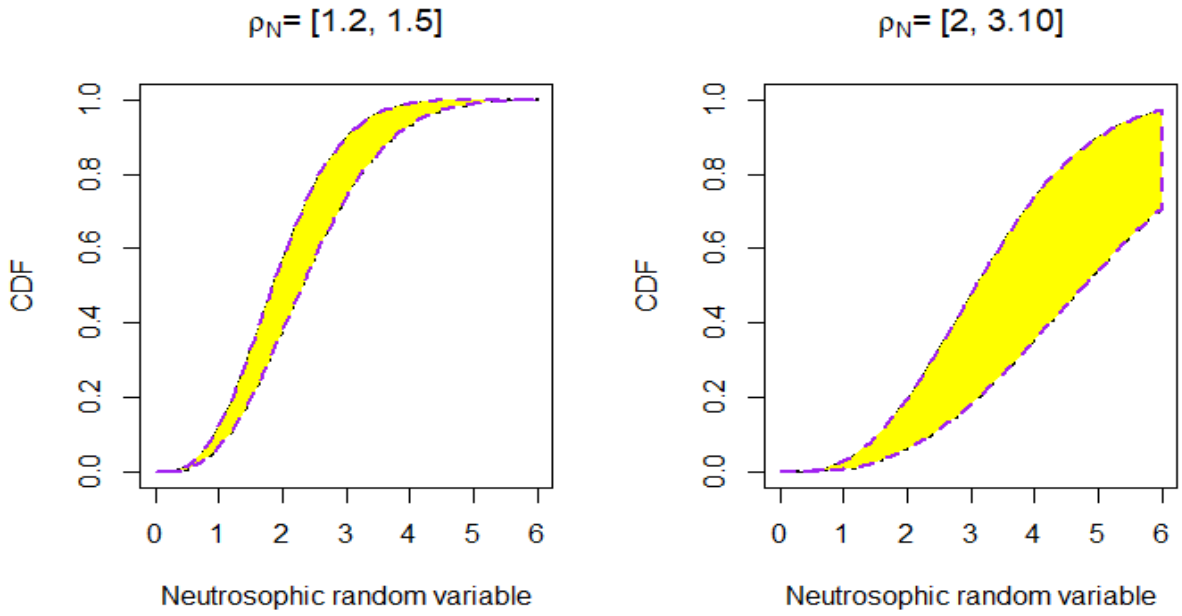

Figure 2. CDF plot of the neutrosophic Maxwell model at different values of ρ_N

DOI: https://doi.org/10.54216/IJNS.270215

Figure 2 shows that as z increases from 0 to infinity, the CDF increases from 0 to 1, accumulating probability. The neutrosophic parameter introduces uncertainty or imprecision into the scale, making the resulting CDF suitable for modeling data with vague or indeterminate attributes, such as those found in uncertain environments or imprecise measurements. The cumulative distribution function is especially useful for computing probabilities, percentiles, and performing inferential statistical analysis with the Maxwell distribution.

Similarly, the related statistics of the neutrosophic Maxwell distribution are given below:

$$\mu_N = 2\frac{\rho_N}{\sqrt{\pi}} \tag{3}$$

$$\sigma_N{}^2 = \left(3 - \frac{8}{\pi}\right)\rho_N^2 \tag{4}$$

where Eq (3) and Eq (4) respectively represent the mean and variance of the neutrosophic Maxwell distribution. Neutrosophic Maxwell distribution's mean and variance are defined based on the uncertain scale parameter. As can be observed, the mean represents the average value of the distribution and takes into account the uncertainty in the system through the application of the neutrosophic scale. Likewise, the variance summarizes the spread (or dispersion) of the data, in this case how far values tend to deviate from their mean when estimated under uncertainty. Incorporating neutrosophic logic, the mean and variance provide a more realistic view of the underlying data when the measurements are vague, incomplete, or imprecise. This makes them particularly advantageous for applications of systems engineering, environmental science, and decision making with uncertainty.

The other related properties of the Maxwell distribution are the shape coefficients, which are given below:

$$\text{Skewness} = \frac{2\sqrt{2}\,(16-5\pi)}{(3\pi-8)^{\frac{3}{2}}} \tag{5}$$

$$\text{Kurtosis} = \frac{4(-96+40\pi-3\pi^2)}{(3\pi-8)^2} \tag{6}$$

Skewness and kurtosis are two important statistics that can give us information about the shape of a dataset. Skewness is the measure of the asymmetry of the distribution that data show with respect to the mean, that is whether the data equally lies on two sides of the mean, while kurtosis is the ratio of the "tailedness" of the distribution of the defined frequency versus a normal distribution being equal to 3 (maximum kurtosis) for a non-tailed distribution. These coefficients explain the dynamics of the distribution, for example probability of exceptionally high values or outliers. For the Maxwell distribution, the values of such coefficients are exact since they arise from a clear mathematical model, where no vague or non-precise parameters are required. The deterministic value for the parameter of neutrosophic Maxwell model is not involved which implies exact values for the skewness and kurtosis of the distribution.

The use of neutrosophic Maxwell and its associated results can be understood by the following example:

Example: If the time taken to complete a certain mechanical process in an industrial setting follows a neutrosophic Maxwell with parameter $\rho_N = [2,4]$, determine the probability that the process would take more than 10 minutes to complete.

Solution: Let Z be a random variable representing required time to complete the process. Then, probability required can be found as given below:

$$P(T > 10) = 1 - H(10; \rho_N) \tag{7}$$

Eq. (7) further can be written as:

$$P(T > 10) = 1 - [H(10; \rho = 2),\ H(10; \rho = 4)] = [0.003,\ 0.143] \tag{8}$$

Thus the neutrosophic probability lies in between 0.3% and 14.3% that the process will take more than 10 minutes, reflecting the uncertainty in the process efficiency due to imprecision in ρ_N.

3. Neutrosophic Maxwell Control Chart

In this section, we present the Shewhart type neutrosophic Maxwell control chart designed for monitoring the shifts in the parameter of neutrosophic Maxwell data generating process.

The structure of neutrosophic VSQ chart is based on the following maximum likelihood estimator of neutrosophic Maxwell distribution:

$$\omega = \sqrt{\frac{\sum_{i=1}^{n} z_{iN}{}^2}{3n}} \tag{9}$$

DOI: https://doi.org/10.54216/IJNS.270215

Eq. (8) can be rewritten as:

$$\omega = \frac{\rho_N}{\sqrt{3m}} T \tag{10}$$

where T is chi random variable with 3-degree of freedom.

The distributional characteristics of the maximum likelihood estimator can be written as:

$$E(\varphi) = \rho_N \varphi \tag{11}$$

$$Var(\omega) = \rho^2{}_N [1 - \varphi^2] \tag{12}$$

where $\varphi = \sqrt{\frac{2}{3n}} \cdot \frac{\Gamma\left(\frac{3n+1}{2}\right)}{\Gamma\left(\frac{3n}{2}\right)}$ is interval form of the neutrosophic constant that depends on neutrosophic sample size.

Two types of control limits are commonly utilized in control chart literature, the k-sigma limits and probability limits. The probability limits of the neutrosophic VSQ chart are given below:

$$UPL = \frac{\rho_N}{\sqrt{3n}} \emptyset_{chi}{}^{-1}\left(1 - \frac{\alpha}{2}\right) \tag{13}$$

$$LPL = \frac{\rho_N}{\sqrt{3n}} \emptyset_{chi}{}^{-1}\left(\frac{\alpha}{2}\right)$$

where $\emptyset^{-1}$ is quantile point of the chi distribution.

Similarly, k-sigma limit can be written as:

$$UCL/LCL = E(\omega) \mp k\sqrt{VarE(\omega)} \tag{14}$$

where k is percentile point of chi distribution.

If we consider, the probability limits, the performance metric of the neutrosophic VSQ chart can be written as:

$$Average\ run\ length\ (ARL) = \frac{1}{1 - \emptyset_{chi}\left(\rho_N \emptyset_{chi}{}^{-1}\left(1-\frac{\alpha}{2}\right)\right) + \emptyset_{chi}\left(\rho_N \emptyset_{chi}{}^{-1}\left(\frac{\alpha}{2}\right)\right)} = \frac{1}{1-\beta} \tag{15}$$

Eq. (15) is used to assess the performance of the neutrosophic chart under in-control and out-of-control chart. It is worth noting that the neutrosophic VSQ chart based on Shewhart model which generally less sensitive to smaller changes in the monitoring parameter. To make it more effective for smaller changes, a new control chart known as neutrosophic exponential weighted moving average control chart is proposed and illustrated in next section.

4. Proposed Control Chart

The development of the proposed MEWMA chart is presented in this section. We consider that the characteristic of the quality to be studied follows a Maxwell distribution form as in equation (1). Assume that we have n imprecise observations of this distribution, and we can write them as $z_1, z_2, \ldots z_n$. Given these kinds of values, a designated statistic, the geometric moving average procedure is given by:

$$T_i = (1 - \gamma) T_{i-1} + \gamma \omega_i; \quad i = 0, 1, \ldots. \tag{16}$$

where ω is neutrosophic plotting statistic. It is worth noting that the indeterminacy is assumed in the distributional parameter of Maxwell distribution not in the coefficient of geometric moving model.

Eq (15) can be written as:

$$\left.\begin{aligned} T_0 &= \omega_0, \\ T_i &= (1 - \gamma)^i T_0 + \textstyle\sum_{j=0}^{i-1} \gamma (1 - \gamma)^j \omega_{(i-j)} \end{aligned}\right\} \tag{17}$$

where the starting value T_0 is the target value ω_0.

Due to the smoothing, a single value becomes less and less important in the test statistic as time goes on (or more data is included). This reduced impact is regulated via the smoothing coefficient γ. The proposed neutrosophic EWMA is more flexible and when smoothing constant is set to 1, it is reduced to traditional VSQ chart. The control limits of the proposed neutrosophic chart can be written as:

$$\left.\begin{aligned} LCL_N &= \rho_N T(n) - k\rho_N \sqrt{\left(\frac{\gamma}{2-\gamma}\right)[1 - (1-\gamma)^{2j}][1 - \varphi^2]} = T_1 \rho_N \\ UCL_N &= \rho_N T(n) + k\rho_N \sqrt{\left(\frac{\gamma}{2-\gamma}\right)[1 - (1-\gamma)^{2j}][1 - \varphi^2]} = T_2 \rho_N \end{aligned}\right\} \tag{18}$$

DOI: https://doi.org/10.54216/IJNS.270215

where k is the correction constant for symmetrically establishing the proposed chart and $T_1 = T(n) - k\sqrt{(\frac{\gamma}{2-\gamma})\,[1-(1-\gamma)^{2j}][1-\varphi^2]}$ and

$T_2 = T(n) + k\sqrt{(\frac{\gamma}{2-\gamma})\,[1-(1-\gamma)^{2j}][1-\varphi^2]}$,

and $LCL_N = min[LCL_l, LCL_u]$ and $= max[UCL_l, UCL_u]$.

The time-varying limits given in (9) fluctuate with j as a function of time. When j is big, the amount $[1-(1-\delta)^{2j}]$tends to one as j gets smaller. Thus, in the case of a larger value of j, we can represent the stable form of control limits as given below:

Eq (17) represents the time varying limits that vary over time, asymptotic form of these limits can be written as:

$$\left.\begin{aligned} LCL_N &= \rho_N T(n) - k\rho_N\sqrt{(\tfrac{\gamma}{2-\gamma})\,[1-\varphi^2]} \\ UCL_N &= \rho_N T(n) + k\rho_N\sqrt{(\tfrac{\gamma}{2-\gamma})\,[1-\varphi^2]} \end{aligned}\right\} \quad (19)$$

In case when actual value of the parameter of neutrosophic Maxwell distribution is not know, the estimated value of the parameter can be used so updated limits can be written as:

$$\left.\begin{aligned} LCL_N &= T_1\hat{\rho}_N \\ UCL_N &= T_2\hat{\rho}_N \end{aligned}\right\} \quad (20)$$

where $\hat{\rho}_N = \frac{\sum_{i=1}^{K}\hat{\omega}_{iN}}{K}$.is grand mean based ok K samples $\hat{\omega}_{iN}$ values.

The values of T_1 and T_2 for different neutrosophic sample sizes and γ are given in Tables 1-2.

Table 1: Factors T_1 and T_2 at $\gamma = 0.05$ for computation of control limits

Time index	Neutrosophic sample					
	[2, 3]		[4,5]		[8,12]	
	T_1	T_2	T_1	T_2	T_1	T_2
1	[0.921,0.941]	[0.997,1.004]	[0.953, 0.960]	[1.006, 1.007]	[0.971, 0.978]	[1.008, 1.008]
2	[0.907, 0.929]	[1.012, 1.016]	[0.943, 0.951]	[1.016, 1.016]	[0.964, 0.972]	[1.014, 1.015]
3	[0.897, 0.921]	[1.022,1.024]	[0.935, 0.944]	[1.022, 1.023]	[0.959, 0.968]	[1.018, 1.020]
4	[0.889,0.914]	[1.030,1.031]	[0.930, 0.940]	[1.027, 1.029]	[0.955, 0.965]	[1.021, 1.024]
5	[0.882,0.909]	[1.036,1.037]	[0.925, 0.935]	[1.031, 1.033]	[0.952, 0.963]	[1.024, 1.027]
6	[0.877,0.905]	[1.041,1.042]	[0.922, 0.932]	[1.035, 1.037]	[0.950, 0.960]	[1.026, 1.030]
7	[0.872, 0.901]	[1.045,1.047]	[0.918, 0.929]	[1.038, 1.040]	[0.947, 0.959]	[1.028, 1.032]
8	[0.868, 0.897]	[1.048,1.051]	[0.916, 0.927]	[1.040, 1.043]	[0.945, 0.957]	[1.029, 1.034]
9	[0.865,0.895]	[1.051,1.054]	[0.913, 0.925]	[1.042, 1.046]	[0.944, 0.956]	[1.031, 1.036]
10	[0.862, 0.892]	[1.053,1.057]	[0.911, 0.923]	[1.044, 1.048]	[0.942, 0.954]	[1.032, 1.037]

DOI: https://doi.org/10.54216/IJNS.270215

Table 2: Factors T_1 and T_2 at $\gamma = 0.05$ for computation of control limits

Time index	Neutrosophic sample					
	[2, 3]		[4,5]		[8,12]	
	T_1	T_2	T_1	T_2	T_1	T_2
1	[0.711, 0.769]	[1.177, 1.208]	[0.802, 0.824]	[1.142, 1.157]	[0.863, 0.890]	[1.096, 1.116]
2	[0.656, 0.724]	[1.222, 1.263]	[0.763, 0.789]	[1.178, 1.196]	[0.836, 0.867]	[1.119, 1.144]
3	[0.632, 0.704]	[1.241, 1.286]	[0.746, 0.774]	[1.193, 1.213]	[0.824, 0.857]	[1.129, 1.156]
4	[0.622, 0.695]	[1.250, 1.297]	[0.738, 0.767]	[1.200, 1.220]	[0.818, 0.853]	[1.133, 1.161]
5	[0.616, 0.691]	[1.254, 1.302]	[0.735, 0.764]	[1.203, 1.224]	[0.816, 0.851]	[1.135, 1.164]
6	[0.614, 0.689]	[1.256, 1.305]	[0.733, 0.762]	[1.205, 1.226]	[0.814, 0.850]	[1.136, 1.165]
7	[0.613, 0.688]	[1.257, 1.306]	[0.732, 0.762]	[1.205, 1.227]	[0.814, 0.849]	[1.137, 1.166]
8	[0.612, 0.687]	[1.258, 1.307]	[0.731, 0.761]	[1.206, 1.227]	[0.813, 0.849]	[1.137, 1.166]
9	[0.612, 0.687]	[1.258, 1.307]	[0.731, 0.761]	[1.206, 1.228]	[0.813, 0.849]	[1.137, 1.166]
10	[0.612, 0.687]	[1.258, 1.307]	[0.731, 0.761]	[1.206, 1.228]	[0.813, 0.849]	[1.137, 1.166]

Tables 1-2, show the values of factors involved in the computation of control limits of the proposed chart. The value of k involved in the computation of T_1 and T_2 can be obtained from the work [12]. This value is selected simulation setup to achieve the in-control (IC) value equal to 370.

5. Performance Evaluation

The performance measures employed in this study are presented in this section. The performance of the proposed control charts is assessed based on various criteria. The average neutrosophic run length (ARL) is the most popular quality characteristic used to evaluate neutrosophic control charts? These curves are then used to study the ability of the control chart in distinguishing between sustained shifts in the process parameters being monitored. The average number of neutrosophic points on the chart before signaling an out-of-control (OC) signal is called the IC average run length (ICARL). Here it is assumed that the samples are regularly spaced. The ICARL is the average number of samples to be taken before a false alarm is given under the stable state. Let the OC average run length, denoted by OCARL, indicate the number of samples in which when the process has been shifted from nominal. An ideal control chart is one with a high ICARL and a low OCARL (to quickly detect process changes). Nevertheless, accomplishing both simultaneously is hard just like balancing Type-I and Type-II error probabilities in testing hypotheses strategy. In order to do this, it is common practice in SPC to set ICARL at a given value and to minimize as much as possible OCARL. Because of similarity with hypothesis testing, we can write the situation in the form of a hypothesis as:

$H_0: \rho_N = \rho_{0N}$; (IC process)

$H_1: \theta = \Delta\rho_{0N} = \rho_{1N}$; (OC process)

In order to compromise, advocates of the theory of control charts often set the value to be some pre-determined value and attempt to drive the value down to a minimum. Here is an approximate formula from Monte Carlo simulation to get the ARL value.

$$ARL_N = \frac{\sum_{i=1}^{K} RL_i}{K} \quad (21)$$

where K is the total number of simulated runs and RL_i is the run length at the ith run. Here, the RL, are samples from time 0 to OC signal triggered by the process. Because the RL is defined by the samples, which are assumed to be uncorrelated and uniformly distributed in time and space, it is expected that for the RL is a random variable.

DOI: https://doi.org/10.54216/IJNS.270215

Applying a simulation method and IC scale parameter equal to $\rho_N = [0.5,1.5]$, we obtained performance indexes quantities for different conditions IC and OOC of Maxwell model. The computed ARL values are given in Figure 3.

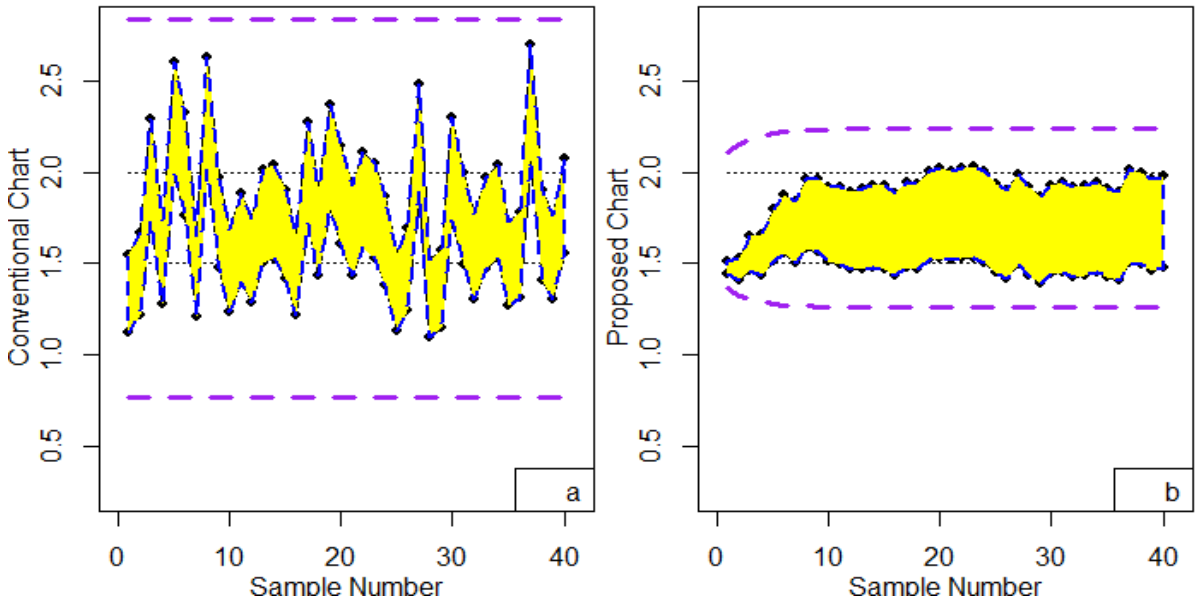

Figure 3. ARL curves of the proposed chart with different parameters setting

Figure 3 displays the performance results (in terms of the ARL) of the proposed chart for a variety of scale parameter shifts. Typically, Figure 3 shows how this ARL changes as the magnitude of the process shift increases. This means that if the ARL curve should drop, as shift increases which is desired and reflected in Figure 3. In neutrosophic framework ARL curve is not a single line curve but a layer where shaded region represents indeterminacy factor.

6. Simulation Analysis

To demonstrate the applicability and practical utility of the proposed chart, we consider simulated data that demonstrates the sensitivity of the chart to small incremental shifts of the parameter of interest. The chart's ability to detect such small changes is confirmed by the simulated data set. We consider the neutrostat R package to simulate a sample of 40 observations from the Maxwell distribution with scale parameter $\rho_N = [1.5, 2]$. These 40 random measurements are shown in Figure4 on conventional neutrosophic version of VSQ chart with ICARL=370 and $n = [5,6]$; also on the proposed chart with ICARL=370, $n = [5,6]$, and $\gamma = 0.15$.

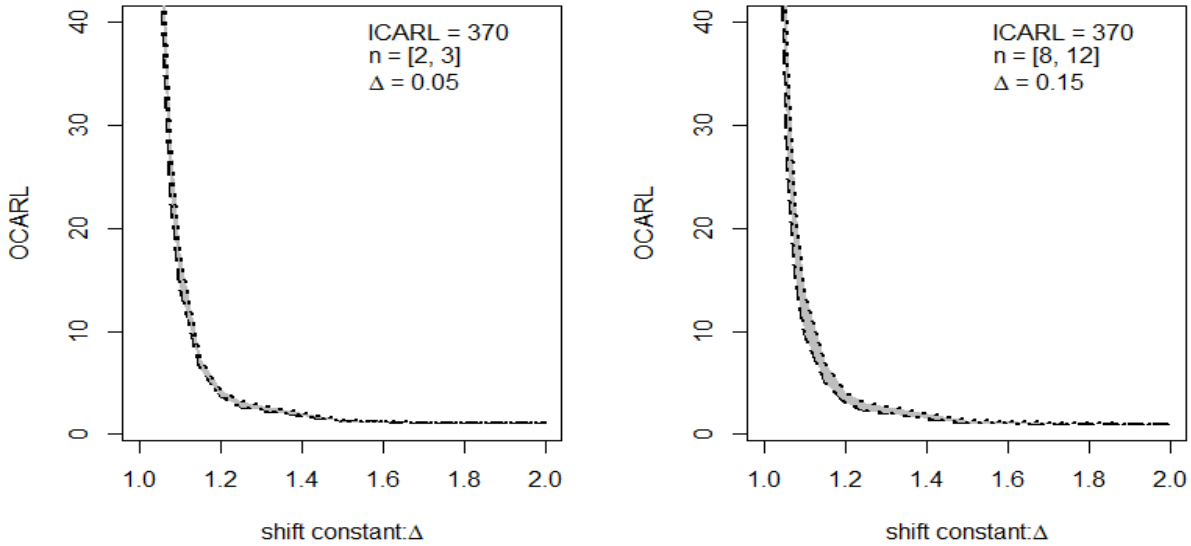

Figure 4. Neutrosophic Maxwell measurements on the (a) existing chart (b) proposed chart

DOI: https://doi.org/10.54216/IJNS.270215

Figure 4 clearly shows that all 40 points lie within the acceptable limits, indicating that the process remains stable and in control. The Figure also displays the upper and lower limits as single lines (not with neutrosophic layer) since it represents the maximum and minimum values of the upper and lower neutrosophic control limits, respectively.

To evaluate the sensitivity of the developed chart, ten new values are again randomly drawn from the Maxwell distribution, but this time with shift constant $\Delta = 1.15$, representing a 15% shift from the target value. Since there has been a 15% change in the observed parameter, these ten values can represent a phase of OC process. The situation is provided in Figure 5.

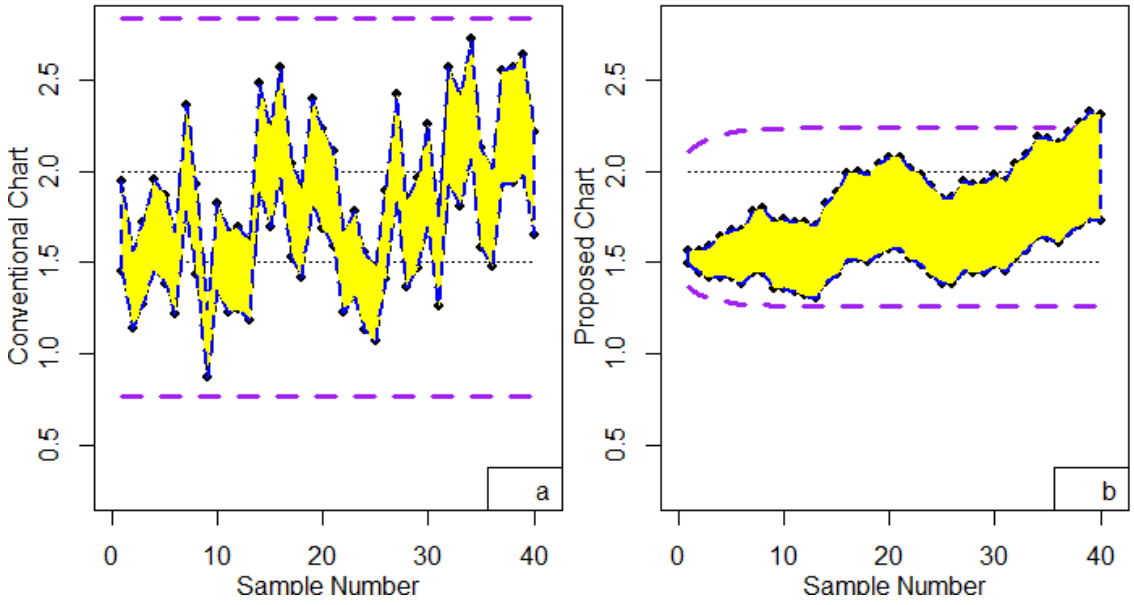

Figure 5. Control chart for out-of-control process

In Figure 5, the presence of anomalous patterns suggests that the system is out of its normal behavior. In Figure 5(b), all the data points after the 30th point are consistently ascending and above the central line which is an obvious indication of OOC state. On the other hand, it is observed in Figure 5(a) that the traditional log-spherical neutrosophic VSQ chart still remains in a state of in-control (IC) and even the small shift is not able to be identified, proving its lesser sensitivity than the proposed chart.

7. Application

In this section, a real data application of the proposed monitoring scheme is presented. For real data analysis, dataset sourced from the work [25], is utilized. The dataset is the first year of complete measurements of solar radiation in Saudi Arabia through a newly established network implemented by the King Abdullah City for Atomic and Renewable Energy (K.A. CARE). The database is composed of minute-to-minute measurements of important solar radiance parameters such as Global Horizontal Irradiance (GHI), Diffuse Horizontal Irradiance (DHI), and Direct Normal Irradiance (DNI) taken from 30 commercial monitoring stations across the country. This spatial and temporal variability needs to be well understood in order to maximize the harnessing of solar energy technologies, particularly in a region that has a wide range of climatic and geographic conditions. Results from [25] indicate significant regional variability, e.g., higher solar irradiance inland compared to the coast and hence photovoltaic and concentrating solar power performance. In order to improve the performance of solar resource assessment and support preventive control we implemented a new monitoring system based on our proposed control chart for the detection of anomalies in the aforementioned measurements of irradiance. This strategy is capable to allow timely detection of anomalous deviations or sensor errors to enhance the data quality and more accurate forecasting, which are essential for effective planning and technology decision-making for the solar energy sector. Due to the inherent uncertainty and variability in the measured solar irradiance data, a neutrosophic-based control chart provides a robust and effective framework for monitoring. Applying this neutrosophic control chart allows for the detection of anomalies and subtle shifts in the data, ensuring improved data quality assurance and more reliable forecasting—both essential for efficient solar energy planning and technology selection. Table 3 presents skewness coefficients of GHI, DNI, and DHI variables for various regions across Saudi Arabia based on the data collected from the KACARE renewable resource atlas. Figure 6 also indicates that the data is positive asymmetric and well suited for Maxwell model.

DOI: https://doi.org/10.54216/IJNS.270215

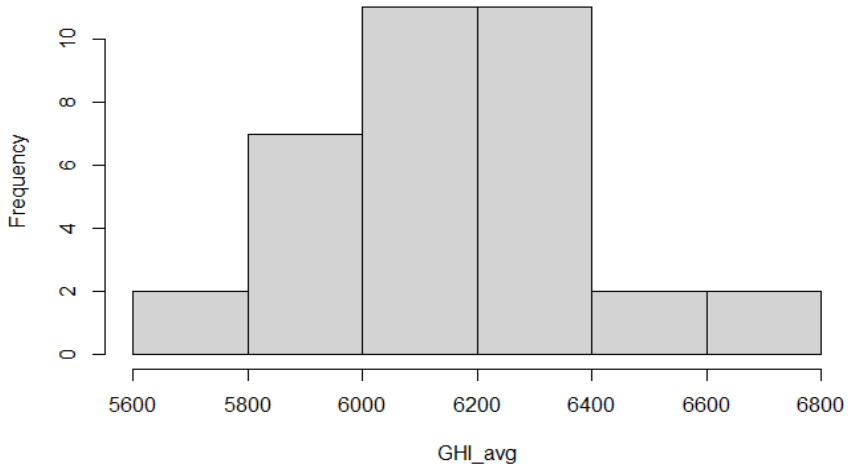

Figure 6. Histogram of the GHI average variable

Table 3: Data Skewness across different radiation data

Solar radiation variable	Skewness coefficient
GHI average	0.355
DNI average	0.326
DHI average	-0.917
GHI max	-0.879
DNI max	-0.439
DHI max	-0.093

An investigation of the skewness analysis is made between different solar radiation in various locations in Saudi Arabia, which reflects different distributional properties in the solar resource in terms of GHI, DNI, and DHI. Some regions such as the Eastern show large positive skewness in all three variables and therefore a skewed distribution, in agreement with the asymmetric distribution of the solar irradiance data. In the Central sector, for instance, the moderate positive skewness can be observed, in particular for DHI, indicating that Maxwell might have a reasonable fit. On the contrary, in areas such as Western Inland the distribution is negatively skewed, indicating a left-skewed distribution less consistent with Maxwell assumption. Hence, considering the above reflections, GHI average variable is the desired level of asymmetry, was chosen for further analysis and implementation of the proposed Maxwell based neutrosophic control chart. The histogram of the GHI average variable is given in Figure 6. This option will guarantee that the chart adequately reflects the asymmetric nature of the irradiance variables and be capable of a sensitive monitoring and detection of the occurs deviation in the solar energy. Since GHI average variable represents the crip values, which is not realistic in this real world, scenerio.It is a key variable in solar energy analysis. It indicates total amount of shortwave solar radiation received per unit area by a horizontal area. The method described by Alduais et al. [12] can be used to create neutrosophic data for the purpose of conceptualizing the proposed control chart.

DOI: https://doi.org/10.54216/IJNS.270215

Table 4: Imprecise GHI averages with computed statistics

Neutrosophic GHI values with uncertainties					ω_i
[6362.29, 6523.75]	[6357.51, 6589.15]	[6232.03, 6502.12]	[6207.29, 6318.85]	[6138.29, 6236.76]	[3614.27, 3715.54]
[6337.25, 6444.39]	[6101.97, 6221.27]	[6054.17, 6300.87]	[6058.8, 6109.67]	[6220.83, 6360.19]	[3553.92, 3630.57]
[6196.02, 6284.3]	[5795.06, 5982.36]	[5719.33, 5798.42]	[6019.69, 6114.37]	[5705.91, 5871.46]	[3400.77, 3471.43]
[5759.49, 5896.24]	[5799.93, 5934.61]	[6649.3, 6803.95]	[6455.8, 6614.08]	[6621.22, 6734.3]	[3619.78, 3700.23]
[5791.43, 5977.98]	[6033.7, 6242.11]	[6111.3, 6225.38]	[5847.62, 6056.79]	[5966.5, 6132.35]	[3435.97, 3537.85]
[5876.49, 6038.98]	[5881.33, 6032.85]	[5982.6, 6166.32]	[6027.48, 6186.82]	[5906.23, 6061.19]	[3426.64, 3520.44]
[6181.28, 6257.34]	[6188.94, 6353.91]	[6218.41, 6467.28]	[6192.03, 6375.67]	[6205.34, 6420.95]	[3577.96, 3680.85]

To construct the proposed control chart, the data was organized into 7 groups, each consisting of 5 observations. The uncertain dataset, along with the corresponding plotting statistics, is presented in Table 4. Table 4 computation based on the sample size is crisp value $n = [5, 5]$, the resulting k value equal to crip number [2.816, 2.816] at $\gamma = 0.15$. The graphical presentation of proposed chart along with plotting statistics is shown in Figure 7.

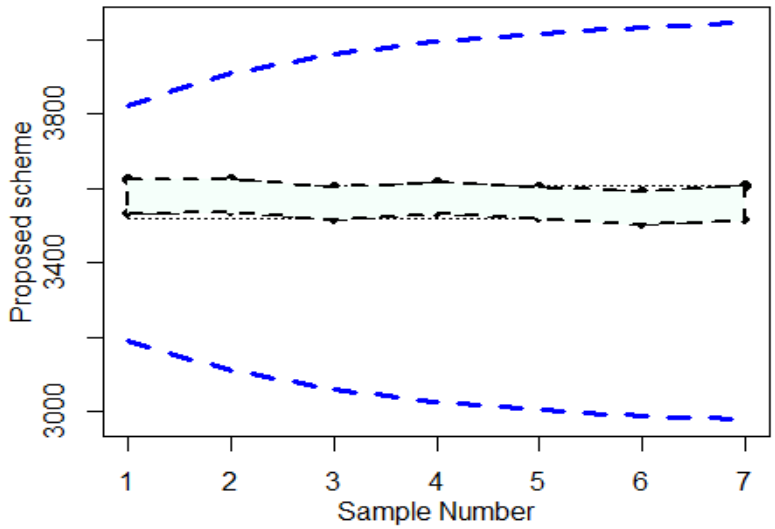

Figure 7. The suggested control chart for solar radiation variable GHI average

Figure 7 indicates that the uncertain GHI average variable remains within the established control limits, suggesting no significant deviation from expected values. As a result, there is no immediate need to implement specific quality control measures or issue signals to data practitioners.

8. Conclusion

In this work, a new control chart has been proposed that aims to assess the variability in Maxwell distributed processes subject to uncertainty in a neutrosophic environment. Extending the existing neutrosophic VSQ chart, this method increases the sensitivity to detect small shifts, which generally are not detectable by classical

DOI: https://doi.org/10.54216/IJNS.270215

Shewhart-type chart by employing the EWMA structure. Extensive run length analysis and Monte Carlo simulations showed that the statistical performance of the chart was satisfactory and that the chart was more efficient for detecting out-of-control signals at different process shifts. The proposed chart has been implemented on simulated data. Numerical results indicate the superior performance of the suggested chart. Furthermore, the treatment of the uncertain GHI with the proposed control chart demonstrates its practical significance and ability to be applied for monitoring real environmental data. The chart accurately reflected the process behavior inside the control limits as expected, which demonstrated the applicability of the proposed method in quality assurance when there is uncertainty in data.

In general, the proposed neutrosophic EWMA-based VSQ chart provides a major contribution to the industries and the fields where precise monitoring of the uncertain, skewed, and Maxwell-distributed data plays a vital role, leading to better process monitoring and decision-making under uncertainty.

Acknowledgement: The authors extend their appreciation to Prince Sattam bin Abdulaziz University for funding this research work through the project number (PSAU/2025/01/ 32758)

Conflicts of Interest: The authors declare no conflict of interest.

References

[1] G. Suman and D. Prajapati, "Control chart applications in healthcare: A literature review," *Int. J. Metrol. Qual. Eng.*, vol. 9, p. 5, 2018.

[2] M. Riaz and F. Muhammad, "An application of control charts in manufacturing industry," *J. Stat. Econometric Methods*, vol. 1, no. 1, pp. 77–92, 2012.

[3] S. A. Yourstone and W. J. Zimmer, "Non-normality and the design of control charts for averages," *Decision Sci.*, vol. 23, no. 5, pp. 1099–1113, 1992.

[4] Y.-C. Lin and C.-Y. Chou, "Non-normality and the variable parameters X control charts," *Eur. J. Oper. Res.*, vol. 176, no. 1, pp. 361–373, 2007.

[5] S. A. Abbasi and A. Miller, "On proper choice of variability control chart for normal and non-normal processes," *Qual. Rel. Eng. Int.*, vol. 28, no. 3, pp. 279–296, 2012.

[6] P. R. Nelson, "Control charts for Weibull processes with standards given," *IEEE Trans. Rel.*, vol. 28, no. 4, pp. 283–288, 2009.

[7] C. W. Zhang, M. Xie, J. Y. Liu, and T. N. Goh, "A control chart for the Gamma distribution as a model of time between events," *Int. J. Prod. Res.*, vol. 45, no. 23, pp. 5649–5666, 2007.

[8] S. Kinat, M. Amin, and T. Mahmood, "GLM-based control charts for the inverse Gaussian distributed response variable," *Qual. Rel. Eng. Int.*, vol. 36, no. 2, pp. 765–783, 2020.

[9] Z. Khan, A. Saghir, A. I. Katona, and Z. T. Kosztyán, "Optimizing P-Chart performance using a percentage-based framework: Application to nonconforming items in the manufacturing sector," *IEEE Access*, 2025.

[10] R. Smith, J. M. Doe, and L. T. Johnson, "A novel approach to control charts using fuzzy logic for quality improvement," *Qual. Eng.*, vol. 36, no. 2, pp. 123–135, 2022, doi: 10.1080/08982112.2022.2034567.

[11] M. Aslam, R. A. R. Bantan, and N. Khan, "Design of a new attribute control chart under neutrosophic statistics," *Int. J. Fuzzy Syst.*, vol. 21, pp. 433–440, 2019.

[12] F. Shah, M. Aslam, and Z. Khan, "New control chart based on neutrosophic Maxwell distribution with decision making applications," *Neutrosophic Sets Syst.*, vol. 53, pp. 297–316, 2023.

[13] Z. Khan, A. Saghir, A. Katona, and Z. T. Kosztyán, "EWMA control chart framework for efficient Maxwell quality characteristic monitoring: An application to the aerospace industry," *Comput. Ind. Eng.*, vol. 200, p. 110753, 2025.

[14] M. P. Hossain, M. H. Omar, and M. Riaz, "New V control chart for the Maxwell distribution," *J. Stat. Comput. Simul*, vol. 87, no. 3, pp. 594–606, 2017.

[15] M. Aslam, A. H. Al-Marshadi, and N. Khan, "A new X-bar control chart for using neutrosophic exponentially weighted moving average," *Mathematics*, vol. 7, no. 10, p. 957, 2019.

[16] R. Alhabib, M. M. Ranna, H. Farah, and A. A. Salama, "Some neutrosophic probability distributions," *Infinite Study*, 2018.

DOI: https://doi.org/10.54216/IJNS.270215

[17] F. Smarandache, *Introduction to Neutrosophic Measure, Neutrosophic Integral, and Neutrosophic Probability*. Infinite Study, 2013.

[18] S. Patel and K. R. Sharma, "Statistical process control in manufacturing: A machine learning perspective," *J. Manuf. Syst.*, vol. 62, pp. 1–10, 2023, doi: 10.1016/j.jmsy.2022.11.004.

[19] M. T. Nguyen and H. L. Tran, "Optimizing quality control processes using hybrid statistical techniques," *Int. J. Prod. Econ.*, vol. 245, p. 108438, 2022, doi: 10.1016/j.ijpe.2021.108438.

[20] M. B. Zeina, M. Abobala, A. Hatip, S. Broumi, and S. J. Mosa, "Algebraic approach to literal neutrosophic Kumaraswamy probability distribution," *Neutrosophic Sets Syst.*, vol. 54, pp. 124–138, 2023.

[21] C. Granados, A. K. Das, and B. Das, "Some continuous neutrosophic distributions with neutrosophic parameters based on neutrosophic random variables," *Adv. Theory Nonlinear Anal. Appl.*, vol. 6, no. 3, pp. 380–389, 2022.

[22] K. F. H. Alhasan and F. Smarandache, *Neutrosophic Weibull Distribution and Neutrosophic Family Weibull Distribution*. Infinite Study, 2019.

[23] S. K. Patro and F. Smarandache, *The Neutrosophic Statistical Distribution, More Problems, More Solutions*. Infinite Study, 2016.

[24] R. A. K. Sherwani, T. Arshad, M. Albassam, M. Aslam, and S. Abbas, "Neutrosophic entropy measures for the Weibull distribution: Theory and applications," *Complex Intell. Syst.*, vol. 7, no. 6, pp. 3067–3076, 2021.

[25] E. Zell *et al.*, "Assessment of solar radiation resources in Saudi Arabia," *Sol. Energy*, vol. 119, pp. 422–438, 2015.

DOI: https://doi.org/10.54216/IJNS.270215